Boundary-Layer Meteorology (2022) 184:531–549
https://doi.org/10.1007/s10546-022-00715-8

RESEARCH ARTICLE

Analysis of Observational Characteristic Features of the Eulerian Autocorrelation Function in Low and Moderate Wind Conditions

Aditya Kumar Dhuria[1] · **Maithili Sharan**[1]

Received: 29 September 2021 / Accepted: 9 May 2022 / Published online: 1 July 2022

Abstract
Turbulent data from three sites are utilized to analyze the characteristic features of the Eulerian autocorrelation function (EAF) of horizontal (longitudinal and lateral) wind components and temperature under different regimes of wind speed and near-surface atmospheric stability. It is shown that classical formulations do not adequately describe the observed EAF behaviour and are unable to capture the peak of the significant negative observed lobe. These formulations are modified by introducing a phase angle α to make them consistent with the observations. The modified formulations are shown to better characterize the behaviour of the EAF curve and its absolute value of significant negative lobe ($|R_{Min}|$) for both low and moderate wind conditions for all three datasets. Further, a new parametrization for the meandering parameter m is proposed in terms of the observed value of $|R_{Min}|$ without using any formulations for the EAF. It is found that the majority of low and moderate wind data belong to the significant meandering range, although the extent of meandering is found to be relatively more pronounced at low wind speeds as compared to moderate wind speeds. The occurrence of meandering (low-frequency horizontal wind oscillations) is found to be independent of stability, topography, and geographical location.

Keywords Autocorrelation coefficient · Low and moderate wind speed · Meandering · Stability

1 Introduction

Weak wind conditions occur in all parts of world but more predominantly in tropical regions. Such conditions assume significance in the study of turbulence characteristics (Agarwal et al. 1995; Yadav et al. 1996). Turbulence may be idealized as consisting of a variety of different-size swirls or eddies, where each eddy behaves in a well-ordered manner when displayed in the form of a spectrum.

✉ Maithili Sharan
mathilis@cas.iitd.ac.in

[1] Centre for Atmospheric Sciences, Indian Institute of Technology Delhi, Hauz Khas, New Delhi 110016, India

The classical exponential function (Taylor 1921) used for the Eulerian autocorrelation function (EAF) describes fully developed turbulence adequately. However, in weak wind, very stable conditions when turbulence is weak and intermittent, the applicability of the classical formulation is questionable. Anfossi et al. (2005) and Moor et al. (2015) have observed significant oscillations in the low-frequency portion of the spectrum of horizontal wind components at low wind speeds. Meandering is an inherent property of the atmosphere, leading to large horizontal wind oscillations, showing a looping behaviour (Anfossi et al. 2005), and is characterized by the presence of large negative lobes in the observed EAF. Anfossi et al. (2005) pointed out that the classical exponential function (Taylor 1921), which adequately describes fully developed turbulence, fails to adequately describe the observed meandering behaviour of the EAF. Various formulations have been proposed in the literature (Frenkiel 1953; Murgatroyd 1969; Philips and Panofsky 1982; Moor et al. 2015) to represent the observed behaviour of EAF under different wind and stability regimes. Anfossi et al. (2005) proposed modified formulations for EAF utilizing the well-known Frenkiel's form for low wind speeds. Moor et al. (2015) suggested a new autocorrelation function to describe the observed negative lobes in the meandering of the horizontal mean wind vector. In order to evaluate the applicability of these formulations and possible modifications, the observed features of the EAF must be analyzed using turbulence observations for a wider range of wind speed and stability regimes.

The effect of wind meandering on pollutant dispersion is that as the wind speed decreases, the hourly-averaged standard deviation of wind direction increases (Sagendorf and Dickson 1974; Sharan et al. 1995, 2003). As a consequence, at low wind speeds it is hard to define a precise plume direction and observed ground-level concentrations may be distributed around 360° in both stable and unstable conditions (Sagendorf and Dickson 1974; Brusasca et al. 1992; Sharan et al. 1996; Anfossi et al. 2006). As a result, the pollution concentration near the source can be overestimated (Sharan et al. 2003) in dispersion models because wind oscillations are not accounted for at low wind speeds. Thus, the meandering patterns characterized by low-frequency motions can play a major role in the horizontal transport of pollutants.

The objective of this study is to analyze the observed behaviour of the EAF using turbulence observations derived from three different sites within the framework of the formulations proposed by Anfossi et al. (2005) and Moor et al. (2015). In addition, an attempt has been made to parametrize the meandering parameter in terms of the magnitude of the observed significant peak of the series of the EAF. Section 2 gives a brief description of experimental datasets of various sites used in the present study. The next section provides the analysis. Results and discussion are given in Sect. 4, and finally, conclusions are summarized in Sect. 5.

2 Description of Datasets

Data from three experimental programs are used in the analysis.

2.1 Ranchi Dataset

The first dataset is from a fast response sonic anemometer installed at 10-m height at the Birla Institute of Technology Mesra, Ranchi (23.4128°N, 85.4408°E), India, with an average elevation 609 m above sea level (http://odis.incois.gov.in/index.php/project-datasets/ctcz-programme/data, Dwivedi et al. 2014). There are few suburban buildings in the area between the east and the north-west. There are hostel buildings, residential houses, and dense trees in the area between the south-east and the east (Tyagi et al.

2012; Dwivedi et al. 2014). The building nearest to the tower is a school to the north-west, with agricultural land in the area between the north-west and the west. The area between the south-east and the west is relatively flat and free from any obstacle (Srivastava and Sharan 2015).

Measurements of three velocity components and temperature at a sampling rate of 10 Hz for the period of one year from January to December 2009 are used in the current study. The data are rotated using the double-rotation method (Wilczak et al. 2000). Data corresponding to mean wind speed $\bar{u} < 0.1$ m s^{-1} are ignored, as the instrument may not be able to respond accurately for such small values. After data quality checking, a total of 5898 hourly data points are selected (Table 1) for further analysis. The diurnal variation of mean wind speed and temperature for the year 2009 is shown in Fig. 1a, d. Here, the continuous curve represents the average values, whereas the vertical error bars indicate deviations from the mean. The average wind speed lies between 1.5 m s^{-1} and 2.9 m s^{-1}, and the standard deviations of

Table 1 Quantitative description of data including number of hours in different wind regimes and stability

Site	Wind					
	Low ($\bar{u} < 2$ m s^{-1})		Moderate (2 m s$^{-1} \leq \bar{u} \leq 6$ m s^{-1})		Strong ($\bar{u} >$ 6 m s^{-1})	
	Stable	Unstable	Stable	Unstable	Stable	Unstable
Ranchi	2981	1704	541	1640	11	21
LASPEX	213	201	54	99	2	7
CASES-99	27	22	199	174	54	78

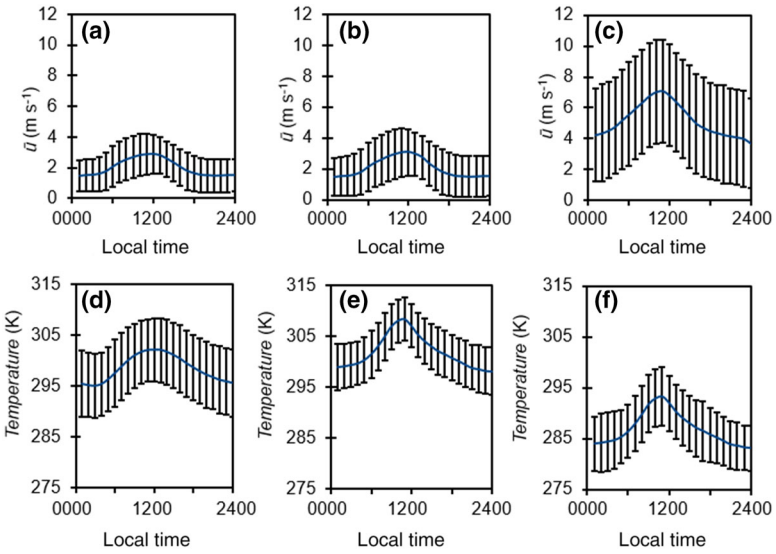

Fig. 1 Diurnal variation of mean wind speed (first row) and temperature (second row) for Ranchi (first column), LASPEX (second column), and CASES99 (third column)

wind speed are in the range of 1.0 m s^{-1} to 1.4 m s^{-1} (Fig. 1a). On the other hand, the average temperature varies from 295 to 303 K with the standard deviations in the range of 6.2 K to 6.6 K (Fig. 1d).

2.2 Land Surface Processes Experiment Dataset

The second dataset is derived from the experiment conducted (Vernekar et al. 2003) from January 1997 to February 1998 in the Sabarmati River basin of Gujarat, which is located in the tropical semi-arid part of the western Indian region. This region is a part of the mainland of Gujarat, India, extending from Runn of Kutch and the Aravalli hills in the north and Damanganga in the south. The mainland is an almost flat plain with an elevation of 45.1 m above mean sea level. Towards the west of this mainland is the peninsular region of Saurashtra, and to the east are hilly tracts at altitudes of 300–600 m (Sheikh 1997; Pandey et al. 2001). Turbulent measurements of velocity and temperature collected from a sonic anemometer with a sampling rate of 10 Hz at 4-m level at Anand (22.35°N, 72.55°E) are used. The climate is semi-arid, and the soil is loamy (Sheikh 1997; Pandey et al. 2001). For the year 1997, the turbulent data were available for the months of February, April, May, June, July, August, October, and December. However, for the year 1998, the data are only available for February. The data are rotated using the double-rotation method (Wilczak et al. 2000). A total of 632 hourly data points are selected after carrying out the quality checks. The average wind speed ranges between 1.5 m s^{-1} and 3.1 m s^{-1} (Fig. 1b), and its standard deviation is in the range of 1.2 m s^{-1} to 1.6 m s^{-1}. On the other hand, the average temperature lies between 298 and 308 K, and its standard deviation is in the range of 4.2 K to 4.7 K (Fig. 1e).

2.3 Cooperative Atmosphere-Surface Exchange Study-1999 Dataset

The third dataset chosen is derived from the CASES-99 (Cooperative Atmosphere-Surface Exchange Study-1999) experiment (Poulos et al. 2002; http://www.eol.ucar.edu/projects/cases99/), which was performed near Leon (37.38°N, 96.14°W) in south-eastern Kansas in the USA during the month of October 1999. The terrain of the main experimental site was relatively flat and homogeneous without any obstacles in the surrounding area. The turbulence measurements were taken on a 60-m tower at 1.5 (0.5)-, 5-, 10-, 20-, 30-, 40-, 50-, and 55-m levels by eight sonic anemometers (CSAT version 3, Campbell Scientific, USA) with a sampling rate of 20 Hz. The turbulence measurements at the 10-m level are used, with data rotated using the double-rotation method (Wilczak et al. 2000). After the quality checking of the data, a total of 554 hourly data points are selected for the analysis (Table 1). The diurnal behaviour of average wind speed and temperature for the period of 6 to 26 October 1999 is shown in Fig. 1c, f. The average wind speed ranges between 4.1 m s^{-1} and 7.0 m s^{-1}, and its standard deviation lies in the range of 2.9 m s^{-1} to 3.4 m s^{-1} (Fig. 1c). On the other hand, the average temperature lies between 284 and 294 K; its standard deviation lies between 4.4 K and 5.8 K (Fig. 1f).

3 Methodology

Datasets from these three sites have been used to study the characteristic features of the EAF. The friction velocity u_* is defined as

$$u_* = [(\overline{u'w'})^2 + (\overline{v'w'})^2]^{\frac{1}{4}}, \tag{1}$$

in which u', v', and w' are the fluctuations in longitudinal, lateral, and vertical velocity components, respectively. The stability parameter ζ is calculated from the expression

$$\zeta = \frac{z}{L} = -\frac{kzg(\overline{w'\theta'_v})}{\bar{\theta}_v u_*^3}, \tag{2}$$

where $\bar{\theta}_v$ is the mean virtual temperature in kelvin, g is the acceleration due to gravity, θ'_v is the fluctuation in the virtual temperature, k is the von Kármán constant, z is the measurement height, and L is the Obukhov length. Based on the mean wind speed, the data are divided into low ($\bar{u} < 2$ m s^{-1}), moderate (2 m s^{-1} $\leq \bar{u} \leq$ 6 m s^{-1}), and strong wind ($\bar{u} > 6$ m s^{-1}) speeds, respectively. Further, the data are subdivided into stable and unstable conditions in accordance with the sign of the stability parameter ζ as positive and negative, respectively. A quantitative description of the data is given in Table 1. In the selected data, there are a relatively small number of strong wind cases (less than 1.5%) from Ranchi and LASPEX (Land Surface Processes Experiment), whereas there are about 24% of strong wind hours in CASES-99. These hours corresponding to strong wind in the Ranchi and LASPEX datasets are considered with those in moderate winds. On the other hand, strong wind hours are dealt separately in CASES-99.

The EAF ($R_x(\tau)$) is defined as

$$R_x(\tau) = \frac{\sum_{i=1}^{n-\tau} (x_i - \overline{x})(x_{i+\tau} - \overline{x})}{\sum_{i=1}^{n} (x_i - \overline{x})^2}, \tag{3}$$

where n is the number of sampling points, τ is the time lag, and x_i are the data points of the series with $\overline{x}$ as its mean. Here x is a generic variable, which can be taken as u, v, w, and θ.

For characterizing the observed behaviour of the EAF of u, v, and θ, various mathematical formulations have been used. Taylor (1921) suggested

$$R_x(\tau) = \mathrm{e}^{\frac{-\tau}{T}}, \tag{4}$$

where T is the turbulent integral time scale. This formulation of $R_x(\tau)$ exhibits a continuously decreasing behaviour with τ and falls to zero for large values of τ. Frenkiel (1953) suggested

$$\mathrm{R}_x(\tau) = \mathrm{e}^{-\frac{\tau}{(m^2+1)T}} \cos \frac{m\tau}{(m^2+1)T}, \tag{5}$$

in which m is a non-dimensional quantity that controls the meandering oscillation frequency (Oettl et al. 2005).

Murgatroyd (1969) expressed Eq. 5 in terms of p and q as

$$R_x(\tau) = \mathrm{e}^{-p\tau} \cos q\tau, \tag{6}$$

where

$$p = \frac{1}{(m^2+1)T}\ ,\ q = \frac{m}{(m^2+1)T}, \tag{7}$$

in which $m = q/p$.

Here the parameters q and p are described in terms of m and T, and their ratio is defined as the loop or meandering parameter m (Anfossi et al. 2005; Mortarini et al. 2016a). The parameter p is related to the turbulence time scale, whereas q is associated with the oscillation time scale. The value of m is crucial to the definition of meandering, because it provides the relative importance of small-scale motions, represented by p, and large-scale motions, represented by q (Mortarini et al. 2013). This implies that meandering is significant for small values of q. We wish to point out that m, p, and q correspond to a generic variable x. Accordingly, in the subsequent text, "suffices u, v, and θ" will represent a quantity corresponding to horizontal (longitudinal and lateral) wind components and temperature.

Philips and Panofsky (1982) proposed an expression for the EAF of the form

$$R_x(\tau) = \frac{1}{(1 + \frac{\tau}{T})^2}. \tag{8}$$

Moor et al. (2015) pointed out that Eq. 8 fails to describe the scalar dispersion in the planetary boundary layer for the low wind conditions when negative lobes are observed in the EAF of the horizontal wind components u and v. Accordingly, Eq. 8 has been modified (Moor et al. 2015) as

$$R_x(\tau) = \frac{\cos q\tau}{(1 + p\tau)^2}. \tag{9}$$

Equations 6 and 9 are used to characterize the negative lobes observed in the EAF curve. In fact, these equations are fitted to the EAF curve to obtain the parameters q and p. The ratio of these two provides the value of m. The absolute value of the significant negative lobe or peak is denoted as $|R_{Min}|$, corresponding to the generic variable x. Henceforth, its value in an EAF curve obtained from the hourly measured time series of the variable x is referred to as the observed $|R_{Min}|$. The peak value of the significant negative lobe in the curve represented by Eqs. 6, 9, 10, and 12 with the fitted values of q and p represents the estimated value of $|R_{Min}|$. The extent of closeness of the estimated value of $|R_{Min}|$ with that observed indicates how well these formulations (Eqs. 6 and 9) are able to characterize the observed behaviour.

A comparison of the magnitudes of observed and computed $|R_{Min}|$ reveals that the peaks of the significant negative lobes computed from Eqs. 6 and 9 are not found to occur at the point of observed peak (Fig. 2a–d) implying a phase shift between them. Also, the computed values of $|R_{Min}|$ are underpredicted in most of the cases. As the computations of p, q, and m are related to the calculation of $|R_{Min}|$, an error in the computation of p, q, and m would lead to an error in computed values of $|R_{Min}|$. Thus, in this analysis, we propose modifying the existing formulations (Eqs. 6 and 9) for incorporating this phase shift for the accurate characterization of the significant negative lobe in the EAF.

The nature of the observed behaviour of the EAF with τ can be considered similar to that observed in the under-damped vibration system where the amplitude of oscillations decays with time (Kelly 2012). Based on the theory of the under-damped vibrational system, the formulation (Eq. 5) for $R_x(\tau)$ can be modified as

$$R_x(\tau) = \mathrm{e}^{-p\tau} \cos(q\tau + \alpha), \tag{10}$$

where the angle α represents a phase difference between two oscillatory curves—one represented by Frenkiel's formula (Eq. 5) and other by the EAF curve obtained from hourly measured time series. It is assumed here that the angle α lies in the first quadrant.

The meandering period (T_*) is defined as

$$T_* = \frac{2\pi}{q}. \tag{11}$$

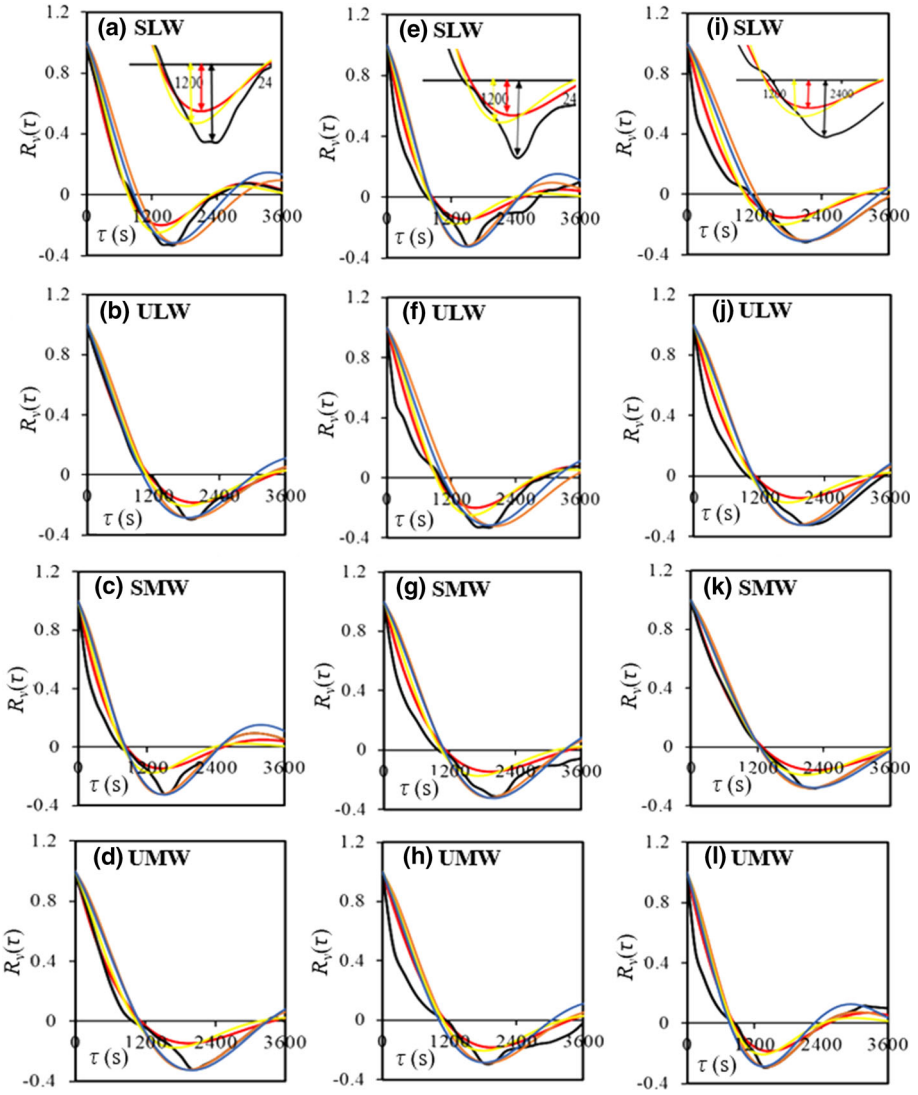

Fig. 2 Variation of $R_v(\tau)$ with τ (s) for Ranchi 2009 Dataset (**a**–**d**), LASPEX (**e**–**h**), and CASES-99 (i–l) represented by first column, second column, and third column, respectively. Graphs for each site are in sequence of stable low wind (SLW), unstable low wind (ULW), stable moderate wind (SMW), and unstable moderate wind (UMW), respectively. Observed (black line), Frenkiel's formula (yellow line), modified Frenkiel's formula (orange line), Moor's formula (red line), and modified Moor's formula (blue line). Length of double arrow in the inserted magnified part (**a**, **e**, **i**) shows the value of significant negative lobe corresponding to observed, Frenkiel's formula, and Moor's formula, respectively

With the similar analogy, Moor's formula (Eq. 9) is modified as

$$R_x(\tau) = \frac{\cos(q\tau + \alpha)}{(1 + p\tau)^2}. \tag{12}$$

These modified formulations are now used to represent the observed behaviour of the EAF in different regimes of mean wind speed and stability. For $\alpha = 0$, Eqs. 10 and 12 are, respectively, reduced to Eqs. 6 and 9. Values of p, q, and α are estimated by fitting Eq. 10 or Eq. 12 to the EAF curve using the generalized reduced gradient nonlinear regression method in Microsoft Excel.

4 Results and Discussion

4.1 Characteristics of Negative Lobes Observed from Different Formulations

The EAF curve for horizontal wind components u and v and temperature θ shows an oscillatory behaviour with the presence of a significant negative lobe, and the amplitude of the oscillations is found to decrease with the time lag τ. Though EAF curves are computed for u, v, and θ, for the sake of brevity, it is shown in the diagram (Fig. 2) for the v component. The corresponding diagrams for u and θ are given in the supplementary material. Four cases such as (i) stable low wind (SLW; Fig. 2a, e, i), (ii) unstable low wind (ULW; Fig. 2b, f, j), (iii) stable moderate wind (SMW; Fig. 2c, g, k), and (iv) unstable moderate wind (UMW; Fig. 2d, h, l) conditions are considered to observe the variation of $R_v(\tau)$ with τ. Estimated values of p, q, and α are given in the supplementary material. The value of α appearing in the table (Table-SM1) is reported in radians in accordance with its units in the cosine function in Eqs. 10 and 12. The corresponding value of α in degrees can be obtained by multiplying with a factor $(180/\pi)$. Values of α in Fig. 2 are found to be in the range of 0.143–0.173 radians (8.19–9.91°) with the modified formulations (Eqs. 10 and 12). With regard to wave motion, a phase shift represents the amount a wave has shifted horizontally from the original wave. Here, there is a phase difference between two oscillatory curves—one represented by Frenkiel's formula (Eq. 5) and the other by the EAF curve obtained from hourly measured series of horizontal wind components u, v, and temperature θ. The original wave (curve represented by Eq. 5) is shifted by an angle to the second wave (represented by Eq. 10). This phase shift is accounted for by the angle α in the modified formulation (Eq. 10), implying that the wave represented by Eq. 5 has been shifted horizontally to the one described by Eq. 10.

The classical formulations (Eqs. 4 and 8) proposed by Taylor (1921) and Philips and Panofsky (1982) exhibit a continuously decreasing exponential behaviour with τ without the presence of any significant negative lobes. The amplitudes of significant negative lobe obtained from Frenkiel's formula (Eq. 5) and Moor's formula (Eq. 9) are underpredicted in the different cases of stability and wind regimes for all the datasets (Fig. 2a–l). The location of the predicted peak in these formulations differs from that observed, implying a phase shift between them (Fig. 2a–l). The inserted magnified diagram around the negative significant lobe is drawn to show the peak and its location corresponding to the observed, Frenkiel's formula and Moor's formula, respectively, for Ranchi (Fig. 2a), LASPEX (Fig. 2e), and CASES-99 (Fig. 2i).

As the existing formulations are unable to predict the $|R_{Min}|$ values accurately, the modified formulations (Eqs. 10 and 12) proposed here by introducing the phase angle α are able to characterize both amplitude and the location of the observed peak (Fig. 2a–l) in a better way. These features are supported in all the four cases of different sites Ranchi (Fig. 2a–d), LASPEX (Fig. 2e–h), and CASES-99 (Fig. 2i–l).

The size of an eddy can be associated with the extent of significant negative lobe on the horizontal τ-axis, which is related to the meandering period T_*. From the computed value

of q, we have calculated T_* (Eq. 11) for each of the EAF curves in Fig. 2. It is found that for Ranchi data, the meandering period is 23 min for the SLW and 23.8 min for the SMW conditions. The corresponding meandering period T_* is 29.3 min and 32.2 min in unstable low wind (ULW) and UMW conditions, respectively. Similarly, in LASPEX, the meandering period T_* is found to be 23.4 min, 30.9 min, 29.6 min, and 32.2 min in low and moderate stable and unstable conditions, respectively. Corresponding values of the period T_* in SLW, SMW, ULW, and UMW in CASES-99 are found to be 34.3 min, 31.3 min, 32.6 min, and 23.9 min, respectively. In the data from Ranchi and LASPEX, the meandering period is found to be more in unstable cases than that with stable conditions. On the other hand, in CASES-99 the value of T_* turns out to be smaller in unstable conditions than the stable stratification in both low and moderate winds. It is hard to draw a conclusion here that the eddies are significantly larger for unstable conditions.

We have also computed the mean meandering period T_* for the whole data classified under low and moderate wind stable and unstable conditions for each site. It is observed that the mean value of period T_* is almost similar for unstable and stable conditions in both low and moderate winds at each site. However, the mean value of T_* is found to be lower in moderate wind than that in low wind conditions.

Scatter diagrams between the magnitudes of observed and computed values of $|R_{Min}|$ for the v-component are shown for the low (Fig. 3a–d) and moderate wind (Fig. 3e–h) conditions for the whole Ranchi dataset considered here. The solid line represents a one-to-one line between the computed and observed values of $|R_{Min}|$ showing ideal behaviour between them, implying that the computed peak of the significant negative lobe of the EAF matches with the observed peak, whereas open circles denote the computed values of $|R_{Min}|$. It is observed that in the majority of the cases, the computed peaks are under-/overpredicted from Eqs. 5 and 9, while in the modified formulations, these are closer to those observed for both low (Fig. 3b, d) and moderate wind conditions (Fig. 3f, h). The root-mean-square error (r.m.s.e.) between observed and computed values of $|R_{Min}|$ is reduced from 0.071 to 0.016 in low wind and 0.044 to 0.01 in moderate wind conditions with the modified Frenkiel's formulation (Eq. 10). The corresponding r.m.s.e. reduces from 0.081 to 0.022 in low wind and from 0.049 to 0.014 in moderate wind conditions with the modified Moor's formula (Table 2). The r.m.s.e. suggests a significant improvement of greater than 70%. A similar inference is drawn from the datasets of LASPEX (Fig. 3i–l) and CASES-99 (Fig. 3m–p). The r.m.s.e. reduces from 0.061 to 0.013 with LASPEX and from 0.058 to 0.013 with CASES-99 in case of modified Frenkiel formula, whereas a similar reduction in r.m.s.e. with modified Moor's formula is found for both LASPEX and CASES-99 (Table 2).

It may be noted that these features are inferred from the analysis of the EAF of the v component of the velocity for different sites and wind conditions. A similar analysis has been carried out for the u-component of the wind and temperature θ, and their diagrams are given in the supplementary material. Similar to the v-component, it is found that (i) the peak of the significant negative lobe computed from the existing formulations of EAF in u (Fig. SM1) and θ (Fig. SM2) is always at some phase angle to the corresponding observed peak and (ii) observed and computed peaks may not occur at the same point. By introducing a phase angle, the computed peak becomes closer to that observed for both u (Figs. SM1 and SM3) and θ (Figs. SM2 and SM4). The corresponding r.m.s.e. is reduced for u and θ from 0.074 and 0.078 to 0.017 and 0.018, respectively, with modified Frenkiel's formulation (Eq. 10) in low wind conditions at Ranchi. The r.m.s.e. values show an improvement by 77–79% in the u-component, 77–78% in the v-component, and 77–79% in the temperature with the modified Frenkiel's formula (Eq. 10) in different wind regimes with all three datasets. In the modified Moor method, the r.m.s.e.s are decreased by 72–74% in the u-component, 73–76% in the

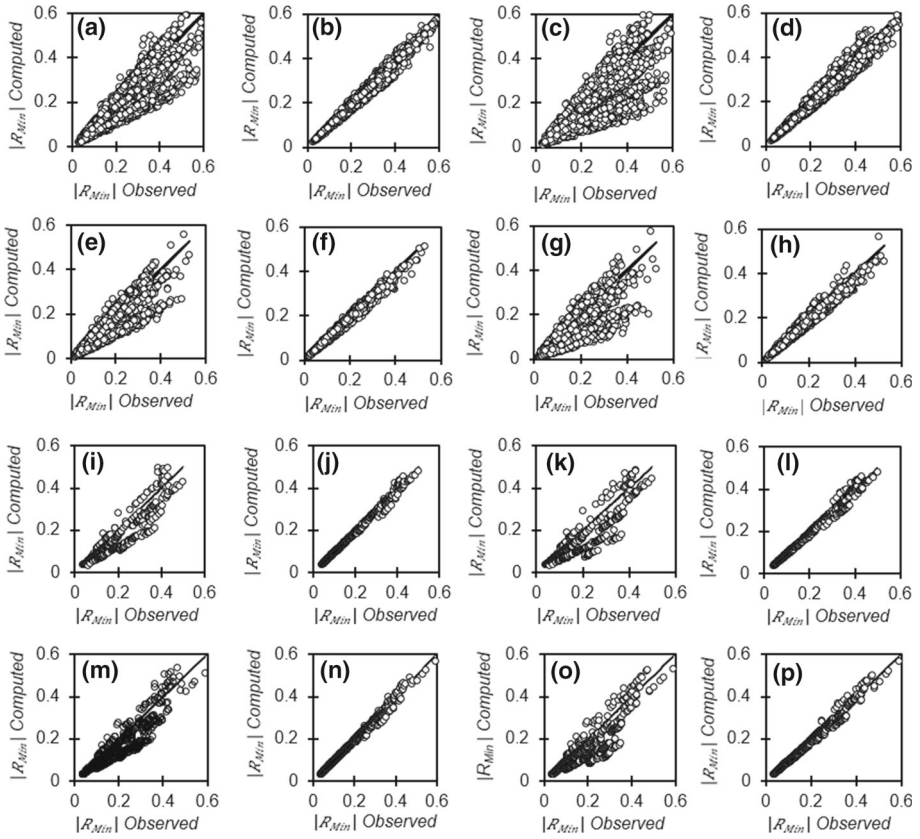

Fig. 3 Variation of computed $|R_{Min}|$ for v component of wind with that observed for low wind Ranchi data (first row), moderate wind Ranchi data (second row), LASPEX (third row), and CASES-99 (fourth row) by using Frenkiel's formula (first column), modified Frenkiel's formula (second column), Moor's formula (third column), and modified Moor's Formula (fourth column). Solid line represents one-to-one line, while the open circles denote the value of computed $|R_{Min}|$. Here observed $|R_{Min}|$ stands for absolute value of the significant negative lobe in an EAF curve derived from hourly measured time series of v component

v-component, and 71–76% in the temperature. Thus, the appreciable reduction in r.m.s.e. (Table 2) shows a significant improvement with both the modified formulations in different wind regimes and stability with all three datasets.

The mean and standard deviation of the phase angle α obtained for the v-component from Eq. 10 and Eq. 12 under different conditions of wind speed and stability for the three sites are given in Table 3. Mean values of α are similar to each other under stable and unstable wind conditions. However, mean values of α under low wind conditions are found to be more comparable to those under moderate wind conditions. Even mean values of α obtained with Eq. 12 are almost similar to those from Eq. 10.

In general, for different datasets, the value of α for the v component in different wind regimes and stability conditions is found to be small and lying in the range 6.3° to 10.3° with both the modified formulations (Eqs. 10 and 12). On the other hand, corresponding values of α are found between 6.1° and 10° for the u component and between 6.2° and 10.1° for the temperature with different datasets. Thus, the modified formulation with the phase angle is

Table 2 Root-mean-square error (r.m.s.e.) between computed and observed values of $|R_{Min}|$ for wind components u, v, and temperature θ for various sites

Site	Variable	Root-mean-square error (r.m.s.e.)			
		Frenkiel's formula	Modified Frenkiel's formula	Moor's formula	Modified Moor's formula
Ranchi (Low wind)	u	0.074	0.017	0.084	0.022
	v	0.071	0.016	0.081	0.022
	θ	0.078	0.018	0.090	0.024
Ranchi (Moderate wind)	u	0.043	0.009	0.048	0.013
	v	0.044	0.010	0.049	0.014
	θ	0.060	0.014	0.067	0.018
LASPEX	u	0.059	0.013	0.066	0.017
	v	0.061	0.013	0.070	0.017
	θ	0.072	0.015	0.083	0.020
CASES-99	u	0.056	0.013	0.064	0.018
	v	0.058	0.013	0.066	0.018
	θ	0.056	0.012	0.063	0.018

able to characterize the observed nature of EAF under different conditions of stability, wind speed, and geographical locations.

4.2 Parametrization of the Meandering Parameter

The meandering parameter m is expressed as the ratio of q and p appearing in Eqs. 10 and 12 for representing the EAF curve. The task here is to do a three-parameter (p, q, α) regression fit of the proposed functional forms (Eqs. 10 and 12) to the EAF curve. Once p and q are known, then m can be found out using Eq. 7. Notice that the parameter m estimated from p and q for u, v, and θ, denoted as m_u,m_v, and m_θ, respectively, can vary for different values of$|R_{Min}|$. Thus, to obtain m, one is required to perform a regression fit with the EAF curve. As the observed peak of the significant negative lobe $|R_{Min}|$ is known from the EAF curve, it is desirable to evolve an empirical relationship between m and observed$|R_{Min}|$.

As p and q can vary for different values of $|R_{Min}|$, m will also vary. Alternatively, empirical relationships between p and $|R_{Min}|$ and q and $|R_{Min}|$ can be developed. However, in practical applications, values of the meandering parameter are often required in spectrum analysis (Mortarini and Anfossi 2015) and air pollution modelling studies (Anfossi et al. 2004). Thus, we have chosen here to formulate an empirical relationship between m and $|R_{Min}|$ to compute m, avoiding the regression fit, for a $|R_{Min}|$ deduced directly as the peak of the significant negative lobe of the EAF curve derived from the observed hourly time series of v. The computed values of $|R_{Min}|$ obtained from modified Frenkiel's formulation (Eq. 10) are relatively close (Table 2) to those observed in comparison with other formulations (Eqs. 6, 9, and 12) for v (Fig. 3b, f, j, n), u (Fig. SM3b, f, j, n), and θ (Fig. SM4b, f, j, n). Thus, the parameter m deduced from the values of p and q obtained from Eq. 10 and the corresponding observed $|R_{Min}|$ values are used for further analysis.

Table 3 Mean and standard deviation of phase angle α (in °) in the modified formulations of Frenkiel and Moor under low and moderate winds for all the three sites

Site	Low wind				Moderate wind			
	Stable low wind		Unstable low wind		Stable moderate wind		Unstable moderate wind	
	Modified Frenkiel	Modified Moor	Modified Frenkiel	Modified Moor	Modified Frenkiel	Modified Moor	Modified Frenkiel	Modified Moor
Ranchi	8.4 ± 1.5	8.4 ± 1.5	8.4 ± 1.5	8.4 ± 1.5	8.1 ± 1.6	8.1 ± 1.6	8.1 ± 1.6	8.1 ± 1.6
LASPEX	8.4 ± 1.6	8.4 ± 1.6	8.4 ± 1.6	8.4 ± 1.6	8.2 ± 1.6	8.2 ± 1.6	8.2 ± 1.6	8.2 ± 1.6
CASES-99	8.3 ± 1.6	8.3 ± 1.7	8.2 ± 1.6	8.2 ± 1.6	8.1 ± 1.7	8.1 ± 1.7	8.1 ± 1.7	8.1 ± 1.7

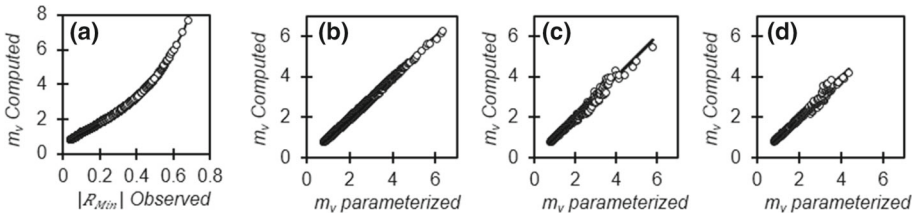

Fig. 4 Variation of computed value of meandering parameter m_v either with the corresponding observed $|R_{Min}|$ for v component or with the value of m_v based on the proposed parametrization for Ranchi. **a** Ranchi data for first six months (January–June 2009). Computed value of m_v is obtained directly from the measurements using the modified formula (Eq. 10). **b** Ranchi data for last six months (July–December 2009); **c** LASPEX; **d** CASES-99. In panels **b**, **c**, and **d**, value of m_v parametrized is computed from the proposed relation between m_v and observed $|R_{Min}|$

For developing the relationship, data for the period from January to June 2009 from the Ranchi site have been used. The meandering parameter m_v is found to increase (Fig. 4a) exponentially with the observed $|R_{Min}|$ and a parametric form for representing their relationship is assumed of the form

$$m_v = c\mathrm{e}^{d|R_{Min}|}, \tag{13}$$

where c and d are the constants obtained using the generalized reduced gradient nonlinear regression method in Microsoft Excel. In theory, a single set of c and d values can be obtained in the entire range of observed $|R_{Min}|$. However, in this case, the accuracy of the proposed relationship reduces significantly for values of $|R_{Min}|< 0.1$. To obtain an accurate representation, the range of $|R_{Min}|$ is divided into six subintervals to estimate the constants c and d appearing in Eq. 13 in each of the corresponding subintervals. Accordingly, these are defined as

$$c = \begin{cases} 0.6205, & \text{when } 0 < |R_{Min}| \le 0.1 \\ 0.8198, & \text{when } 0.1 < |R_{Min}| \le 0.2 \\ 0.9597, & \text{when } 0.2 < |R_{Min}| \le 0.3 \\ 1.0286, & \text{when } 0.3 < |R_{Min}| \le 0.4 \\ 1.0205, & \text{when } 0.4 < |R_{Min}| \le 0.5 \\ 0.9070, & \text{when } 0.5 < |R_{Min}| < 0.6 \end{cases}, \tag{14a}$$

$$d = \begin{cases} 6.9310, & \text{when } 0 < |R_{Min}| \le 0.1 \\ 3.9507, & \text{when } 0.1 < |R_{Min}| \le 0.2 \\ 3.1203, & \text{when } 0.2 < |R_{Min}| \le 0.3 \\ 2.9030, & \text{when } 0.3 < |R_{Min}| \le 0.4 \\ 2.9109, & \text{when } 0.4 < |R_{Min}| \le 0.5 \\ 3.1593, & \text{when } 0.5 < |R_{Min}| < 0.6 \end{cases}. \tag{14b}$$

The parametrization (Eq. 13) is tested on the data for the remaining period of six months (July–December 2009) from the Ranchi dataset. It is found that the value of m_v calculated from the proposed formulation (Eq. 13) is found to be close to that computed from Eq. 10. The maximum absolute error in the meandering parameter is calculated by taking the difference between the values computed from the proposed parametrization (Eq. 13) and those obtained from the modified formulation (Eq. 10). The maximum absolute percentage error is deduced

from the formula

$$MAPE = Max \frac{|m_v(Eq.13) - m_v(Eq.10)|}{m_v(Eq.10)} \times 100. \quad (15)$$

For the period of July–December 2009, the maximum absolute percentage error with the constants c and d (Eq. 14a and b) is found to be 1.93% for the v component of wind.

Now we examine the performance of the proposed parametrization (Eq. 13) if it is used with the same coefficients c and d (Eq. 14a and b) for computing the parameters m_u and m_θ from the values of observed $|R_{Min}|$ corresponding to u and θ. For this evaluation, the u-component of the wind and temperature θ from the turbulence data at Ranchi for the period of one year (January–December 2009) are used. As described earlier, values of m_u and m_θ based on Eq. 10 are calculated for each hour corresponding to the values of observed $|R_{Min}|$ for u and θ. These observed values of $|R_{Min}|$ are also used to compute values of m_u and m_θ from the proposed parametrization (Eq. 13). The values computed from this parametrization (Eq. 13) are found to be in good agreement with those obtained from the parameters p and q calculated using Eq. 10 for u-component and θ. The maximum absolute percentage error in using the proposed relation for u-component is found to be 1.8%. The corresponding error in the case of θ is found to be 2.0%. Thus, the proposed relationship can be used for deducing the values of meandering parameters by simply knowing the magnitude of the amplitude of observed significant negative lobe in the EAF curve.

The performance of the proposed parametrization (Eq. 13) is also evaluated with the observations from the LASPEX and CASES-99 experiments for the parameters m_u, m_v, and m_θ. The maximum absolute percentage error in the computation of these parameters is found to be 3.0% for LASPEX and 3.3% for CASES-99. In totality, the parametrization (Eq. 13) proposed here is able to predict the meandering parameter reasonably accurately for u, v, and θ directly by taking the corresponding observed absolute value of significant negative lobe in the time series of turbulence data under different conditions of wind speed and stability. As the proposed parametrization for the meandering parameter is dependent only on the magnitude of the observed significant negative lobe and does not involve the uncertainties associated with underlying computation, we expect that this will provide a reasonable estimate for m_u,m_v, and m_θ under various conditions.

4.3 Frequency of Meandering

In the last section, a new parametrization was proposed for computing the meandering parameter from the observed value of significant negative lobe. As this parametrization is dependent on the observed value of negative significant lobe and not on the computed one, it is expected to be more reliable and accurate to show the extent of meandering in any particular hour of the datasets. Values of the meandering parameters are often required in spectrum analysis and air pollution modelling studies (Anfossi et al. 2004). Mortarini and Anfossi (2015) have analysed the turbulence measurements taken at the Graz and Tisby Site and classified the data into meandering and non-meandering cases depending on the values of both m_u and m_v if these are larger or smaller than one. Recently, Mortarini et al. (2016b) classified the meandering and non-meandering cases based on the values of parameters m_u,m_v, and m_θ such that (i) there is no meandering when all m_u,m_v, and m_θ are less than 1; (ii) meandering begins when at least one m_u,m_v, or m_θ is greater than 1; and (iii) there is significant meandering when all m_u,m_v, and m_θ are greater than 1. We have adopted their proposition in the present study to distinguish between meandering and non-meandering cases. Accordingly,

Table 4 Low wind data classified into different classes of meandering (no meandering, beginning of meandering, and significant meandering)

Site	Total No. of low wind cases	No meandering cases		Beginning of meandering cases		Significant meandering cases	
		No. of Hours	% of total	No. of Hours	% of total	No. of Hours	% of total
Ranchi	4685	2	0.04	496	10.59	4191	89.46
LASPEX	414	1	0.24	59	14.25	354	85.51
CASES-99	49	0	0.00	1	2.00	48	97.96

Table 5 As Table 4 but for moderate wind

Site	Total No. of Moderate wind cases	No meandering cases		Beginning of meandering cases		Significant meandering cases	
		No. of Hours	% of total	No. of Hours	% of total	No. of Hours	% of total
Ranchi	2181	13	0.60	491	22.51	1677	76.89
LASPEX	153	0	0.00	41	26.80	112	73.20
CASES-99	373	17	4.56	49	13.14	307	82.31

the turbulence data have been classified into three groups based on the values of m_u,m_v, and m_θ.

The quantitative distribution of the low and moderate wind data at various sites into three different classes based upon the values of the parameters m_u,m_v, and m_θ is presented in Tables 4 and 5, respectively. To reveal the extent of meandering in the whole dataset, pie charts (Fig. 5a–c) are presented for different sites. From the pie chart (Fig. 5a) for the Ranchi dataset, it is seen that most of the data lie in the significant meandering range for both low and moderate wind conditions. There are about 4685 number of low wind cases in the Ranchi dataset, out of which 4191 lie in the significant meandering range. Similarly, out of 2213 moderate wind cases, around 1677 lie in the significant meandering range. Thus, Table 4 and Fig. 5a reveal that the majority of the low and moderate wind cases in Ranchi data fall in the significant meandering class.

A similar trend is observed in the LASPEX and CASES-99 datasets as well. While for the LASPEX dataset (Fig. 5b), 354 out of 414 low wind hours and 112 out of 153 moderate wind hours fall in the significant meandering range. For the CASES-99 site (Fig. 5c), 48 out of 49 low wind cases and 307 out of 373 moderate wind cases lie in the significant meandering range. In CASES-99, there are 23.8% cases corresponding to strong wind. However, all the strong wind cases are found to fall in the non-meandering category (Fig. 5c) as the values of observed $|R_{Min}| < 0.07$ in the EAF curves and the meandering parameter $m < 1$ for horizontal wind components u and v and temperature θ. Each of the colours in Fig. 5 includes both stable and unstable cases. The CASES-99 data have a relatively low occurrence of low wind significant meandering (Fig. 5).

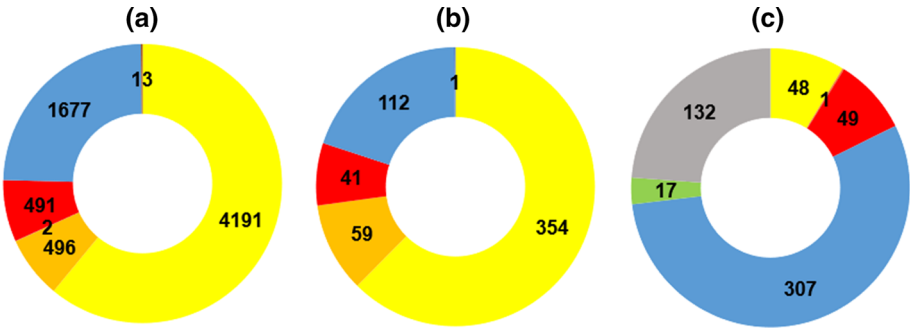

Fig. 5 Pie chart depicting frequency distribution of low and moderate wind data into different classes of meandering for **a** Ranchi data, **b** LASPEX data, **c** CASES-99 data. Numbers on the pie chart signify the cases lying in a particular frequency class. Low wind (SLW and ULW) no meandering (purple), low wind (SLW and ULW) beginning of meandering (golden brown), low wind (SLW and ULW) significant meandering (yellow), moderate wind (SMW and UMW) no meandering (green), moderate wind (SMW and UMW) beginning of meandering (red), moderate wind (SMW and UMW) significant meandering (blue), strong wind (SSW and USW) no meandering (silver)

The maximum number of cases is found to fall (Tables 4, 5) in the third category (significant meandering) for all the datasets under different wind regimes, implying the occurrence of significant meandering in both low and moderate wind conditions, although the extent of meandering is relatively high in the low winds for the different datasets. This conclusion for moderate wind differs from that reported by Mortarini and Anfossi (2015) and Mortarini et al. (2016b). They noticed the occurrence of significant meandering in the cases corresponding to low wind (< 1.5 m s^{-1}) conditions only and did not observe significant meandering in the moderate wind (> 1.5 m s^{-1}) cases. Mortarini et al. (2016b) found that in moderate wind (> 1.5 m s^{-1}), the maximum number of cases falls in the first category corresponding to no meandering. This may be due to the fact that Frenkiel's formula (Eq. 5) used by Mortarini and Anfossi (2015) and Mortarini et al. (2016b) underpredicts (Fig. 3a, e, i, m) the value of significant negative lobe $|R_{Min}|$ in the EAF data resulting in the under-prediction of parameters m_u,m_v, and m_θ.

We have also quantified the data in low and moderate winds for different sites based on the absolute value of $|R_{Min}|$ in the EAF curves of u, v, and θ. It is observed that the value of $|R_{Min}|$ equals 0.07, corresponding to $m_u = m_v = m_\theta = 1$. We have divided the low and moderate wind data into different classes of meandering based on the values of $|R_{Min}|$ such that (i) no meandering occurs when all of $|R_{Min}|$ values for u, v, and θ are less than 0.07; (ii) meandering begins when at least one of $|R_{Min}|$ values for u, v, and θ are greater than 0.07; and (iii) significant meandering occurs when all of $|R_{Min}|$ values for u, v, and temperature θ are greater than 0.07.

5 Conclusions

The observed characteristics of EAF for horizontal wind components u, v, and temperature θ are analysed for three different sites under different conditions of wind speed and stability. It is found that the existing formulations (Eqs. 5 and 9) are unable to characterize the observed features of the EAF. These formulations are unable to predict accurately the $|R_{Min}|$ values for u, v, and θ. In addition, there is a difference between the observed and computed peaks of

the EAF, indicating a phase shift between them. An attempt has been made to bridge the gap between the observed and computed behaviour of EAF by incorporating a phase angle α in the formulations. The modified formulations (Eqs. 10 and 12) with the inclusion of phase angle are able to characterize the behaviour of the observed EAF curve relatively better. Further, the observed $|R_{Min}|$ values for u, v, and θ can be predicted with relatively better accuracy. The modified formulations lead to significant reduction in the r.m.s.e. between the observed and computed values of $|R_{Min}|$ for u, v, and θ indicating that the modified formulations are able to better predict the values of $|R_{Min}|$ compared to the existing formulations.

A parametrization for computing the meandering parameter m for u, v, and θ directly from the observed values of $|R_{Min}|$ is made and tested on different datasets for different wind speeds and stability. This parametrization is able to compute the m values directly from the observed values of $|R_{Min}|$ up to the accuracy of 98% for all the three sites without using any existing formulation for it. So, the extent of meandering can be computed directly using the observed $|R_{Min}|$ values for u, v, and θ.

The quantitative distribution of the data is assessed between meandering and non-meandering cases using the computed values of meandering parameters m_u,m_v, and m_θ. It is found that the majority of cases for all the three sites are found in the significant meandering range indicating the presence of significant meandering in both low and moderate wind conditions, although the extent of meandering is more significant in the low wind as compared to moderate wind.

Thus, the study suggests that the significant negative lobes in the EAF curves of u, v, and θ are observed in both low and moderate wind conditions of different datasets. A majority of the low and moderate wind data lies in the significant meandering range for all the datasets. Also, the significant negative lobe in the EAF curve of the vertical component of wind was not observed in all the dataset, and thus, the occurrence of meandering effect is presumed in the horizontal wind components.

In most of the studies, the mean wind speed of 2 m s^{-1} is used for separating the data into low and moderate wind cases. We wish to point out that by considering a threshold value of mean wind speed as 1.5 m s^{-1} for separating the low and moderate wind cases as done by Anfossi et al. (2004), some of the low wind cases in the range of 1.5–2 m s^{-1} shift into the class of moderate wind, further supporting the occurrence of significant meandering in both low and moderate wind conditions. Although the extent of meandering is observed to be relatively greater in low wind conditions as compared to that in moderate winds, the meandering effect in moderate wind conditions cannot be ignored and should be taken in account.

In the present study, data from three different sites are considered for the analysis. The mean wind speed is appreciably larger at CASES-99 (Fig. 1) than that at the other two sites. Besides, the anemometer used in LASPEX is at 4-m height, while in the other two they are at 10 m. The number of cases in low, moderate, and strong wind conditions in LASPEX (Table 1) could be different if the measurements were at 10-m height. Low-frequency flow processes, such as meandering, may be influenced by surface heterogeneity (Mortarini et al. 2016b).

The observed significant negative lobe for convective conditions (especially in the unstable low-wind regime) may be associated with large-scale circulations embracing the entire convective boundary layer rather than meandering motions. These random convective boundary layer-scale coherent structures produce random gusts in the layer attached to the bottom of the large eddies. The typical time scale of these large-scale eddies could be ~ Z_i/w_* ~ 10–20 min (here Z_i is the convective-boundary-layer height and w_* is the Deardorff 1970 convective velocity scale), and its value lies between 10–20 min. However, the time scales

associated with the observed significant negative lobe in Fig. 2 are found to be in range of 29–32.6 min in low wind and 24–32 min in moderate wind unstable conditions. In all the three datasets, it is found that more than 93% of hours have a meandering period in the range of 20–35 min. The meandering oscillations are usually associated with the stable boundary layer. Analysis of the Deardorff's time scale for the convective-boundary-layer cases as well as the Brunt–Väisälä frequency for the stable-boundary-layer cases to better understand the nature of negative lobe will be taken up with the availability of required data.

Supplementary Information The online version contains supplementary material available at https://doi.org/10.1007/s10546-022-00715-8.

Acknowledgements The authors wish to thank Dr. Manoj Kumar for providing observational data for Ranchi, Indian Institute of Tropical Meteorology Pune for the LASPEX dataset and National Center for Atmospheric Research (NCAR) for CASES-99 observations. Authors thank Dr. Piyush Srivastava for his valuable suggestions. We would also like to thank the reviewers for their valuable comments. The authors declare no competing interests. The turbulence data used in this study can be obtained for Ranchi from the Indian National Centre for Ocean Information Services (http://www.incois.gov.in/portal/datainfo/ctczdata.jsp) upon request and for CASES-99 from the site http://www.eol.ucar.edu/projects/cases99/.

References

Agarwal P, Yadav A, Gulati A, Raman S, Rao S, Singh M, Nigam S, Reddy N (1995) Surface layer turbulence processes in low wind speeds over land. Atmos Environ 29:2089–2098

Anfossi D, Oettl D, Degrazia G (2004) Some Aspects of Turbulence and Dispersion in Low Wind Speed Conditions. Air Pollution Modelling and Its Application XVI. Springer, Boston, MA. https://doi.org/10.1007/978-1-4419-8867-6_30

Anfossi D, Oettl D, Degrazia G, Goulart A (2005) An analysis of sonic anemometer observations in low wind speed conditions. Boundary-Layer Meteorol 114:179–203

Anfossi D, Alessandrini S, Trini S, Ferrero E, Oettl D, Degrazia G (2006) Tracer dispersion simulation in low wind speed conditions with a new 2-D Langevin equation system. Atmos Environ 40:7234–7245

Brusasca G, Tinarelli G, Anfossi D (1992) Particle model simulation of diffusion in low wind speed stable conditions. Atmos Environ 26 A:707–723

Deardorff J (1970) Preliminary results from numerical integrations of the unstable boundary layer. J Atmos Sci 27:1209–1211

Dwivedi A, Chandra S, Kumar M, Kumar S, Kumar N (2014) Spectral analysis of wind and temperature components during lightning in pre-monsoon season over Ranchi. Meteorol Atmos Phys 127:95–105

Frenkiel F (1953) Turbulent Diffusion: Mean Concentration Distribution in a Flow Field of Homogeneous Turbulence. Adv Appl Mech 3:61–107

Kelly S (2012) Mechanical Vibrations: Theory and Applications, Cengage Learning: 672

Kumar P, Sharan M (2012) An analysis for the applicability of Monin-Obukhov similarity theory in stable conditions. J Atmos Sci 69:1910–1915

Moor L, Degrazia G, Stefanello M, Mortarini L, Acevedo O, Maldaner S, Szinvelski S, Roberti D, Buligon L, Anfossi D (2015) Proposal of a new autocorrelation function in low wind speed conditions. Physica A 438:286–292

Mortarini L, Ferrero E, Falabino S, Trini S, Richiardone R, Anfossi D (2013) Low-frequency processes and turbulence structure in a perturbed boundary layer. Q J R Meteorol Soc 139:1059–1072. https://doi.org/10.1002/qj.2015

Mortarini L, Anfossi D (2015) Proposal of an empirical velocity spectrum formula in low-wind speed conditions. Q J R Meteorol Soc. https://doi.org/10.1002/qj.2336

Mortarini L, Maldaner S, Moor L, Stefanello M, Acevedo O, Degrazia G, Anfossi D (2016a) Temperature Auto-correlation and Spectra functions in low-wind meandering conditions. Q J R Meteorol Soc 142:1881–1889. https://doi.org/10.1002/qj.2796

Mortarini L, Stefanello M, Degrazia G, Roberti D, Castelli S, Anfossi D (2016b) Characterization of wind meandering in low wind conditions. Boundary-Layer Meteorol 161:165–182. https://doi.org/10.1007/s10546-016-0165-6

Murgatroyd R (1969) Estimations from Geostrophic Trajectories of horizontal diffusivity in the mid-latitude troposphere and lower stratosphere. Q J R Meteorol Soc 95:40–62
Oettl D, Goulart A, Degrazia G, Anfossi D (2005) A new hypothesis on meandering atmospheric flows in low wind speed conditions. Atmos Environ 39:1739–1748
Phillips P, Panofsky H (1982) A re-examination of lateral dispersion from continuous sources. Atmos Environ 16:1851–1859
Pandey V, Kumar M, Sheikh A (2001) Agroclimatic features of LASPEX sites. J Agrometeorol 3:39–55
Poulos G, Blumen W, Fritts D, Lundquist J, Sun J, Burns S (2002) CASES-99: A comprehensive investigation of the stable nocturnal boundary layer. Bull Am Meteorol Soc 83:555–581
Sagendorf J, Dickson D (1974) Diffusion under low wind speed inversion conditions. NOAA Technical memoerl-arl-52. Technical report, Air Resources Laboratories, Silver Spring, MD
Sharan M, Modani M, Yadav A (2003) Atmospheric dispersion: an overview of mathematical modelling framework. Proc Indian National Science Academy Part A Phys Sci 69:725–744
Sharan M, Srivastava P (2016) Characteristics of heat flux in unstable atmospheric surface layer. J Atmos Sci 73:4519–4529
Sharan M, Yadav A, Singh M (1995) Comparison of various sigma schemes for estimating dispersion of air pollutants in low winds. Atmos Environ 29:2051–2059
Sharan M, Yadav A, Singh M (1996) A time dependent mathematical model using coupled puff and segmented approaches. J Appl Meteorol 35:1625–1631
Sheikh A (1997) Agroclimatic Atlas of Gujarat. Gujarat Agricultural University, Anand, India
Taylor G (1921) Diffusion by continuous movements. Proc London Math Soc Ser 2(20):196–211
Tyagi B, Satyanarayana A, Kumar M, Mahanti N (2012) Surface energy and radiation budget over a tropical station: An observational study. Asia-Pac J Atmos Sci 48:411–421. https://doi.org/10.1007/s13143-012-0037-z
Vernekar K, Sinha S, Sadani L, Sivramakrishnan S, Parasnis S, Brij M, Saxena S, Dharamraj T, Patil M, Pillai J, Murthy B, Debaje S, Bagavatsingh A (2003) An overview of the Land Surface Processes Experiment (LASPEX) over a semi-arid region of India. Boundary-Layer Meteorol 106:561–572
Wilczak J, Oncley S, Stage S (2001) Sonic anemometer tilt correction algorithms. Boundary-Layer Meteorol 99:127–150
Yadav A, Sethuraman SM (1996) Surface layer turbulence spectra and eddy dissipation during low winds in tropics. Boundary-Layer Meteorol 79:205–224